Low-energy ω ($\rightarrow \pi^0\gamma$) meson photoproduction in the nucleus

Swapan Das*

Nuclear Physics Division, Bhabha Atomic Research Centre, Mumbai 400085, India

(Received 20 October 2010; revised manuscript received 7 April 2011; published 20 June 2011)

The $\pi^0\gamma$ invariant mass distribution spectra in the $(\gamma, \pi^0\gamma)$ reaction were measured by the TAPS/ELSA Collaboration to look for the hadron parameters of the ω meson in the Nb nucleus. We study the mechanism for this reaction, where we consider that the elementary reaction in the Nb nucleus proceeds as $\gamma N \rightarrow \omega N; \omega \rightarrow \pi^0\gamma$. The ω-meson photoproduction amplitude for this reaction is extracted from the measured four-momentum transfer distribution in the $\gamma p \rightarrow \omega p$ reaction. The propagation of the ω meson and the distorted wave function for the π^0 meson in the final state are described by the eikonal form. The ω and π^0 mesons' nucleus optical potentials, appearing in the ω meson propagator and π^0 meson distorted wave function respectively, are estimated using the $t\varrho$ approximation. The effects of pair correlation and color transparency are also studied. The calculated results do not show medium modification for the ω meson produced in the nucleus for momentum greater than 200 MeV. It occurs because the ω meson predominantly decays outside the nucleus. The dependence of the cross section on the final-state interaction is also investigated. The broadening of the ω-meson mass distribution spectra is shown to occur due to the large resolution width associated with the detector used in the experiment.

DOI: 10.1103/PhysRevC.83.064608 PACS number(s): 25.20.Lj, 13.60.Le

I. INTRODUCTION

The study of the properties of vector meson in the nuclear medium is a topic of intense interest in the nuclear physics. This topic has been pursued vigorously in recent years to determine quantitatively the mass and width of the vector meson in the nucleus. Various model calculations relate the in-medium properties of vector meson with the chiral symmetry in QCD. The restoration of this symmetry in the nuclear medium predicts the reduction of the vector meson mass, which could be drastic in the hot and/or dense nuclear medium [1]. Using the scaling property in QCD, Brow and Rho [2] have shown that the vector meson mass should drop in the nuclear medium. Other model calculations, such as the QCD sum rule calculations by Hatsuda *et al.* [3], Vector Meson Dominance (VMD) model calculations by Asakawa *et al.* [4], and the quark meson coupling model calculations by Saito *et al.* [5], corroborate this finding. On the other hand, vector meson mass shift (upward) and width broadening in the hot and dense nuclear matter have also been reported [6].

Large medium modification of the ρ meson was indicated first in the enhanced dilepton yield (between 300 and 700 MeV) in CERES and HELIOS ultrarelativistic heavy-ion collision data taken sometime around 1995 in CERN-SPS [7]. The quantitative estimation of this modification could not be made in that time because of the poor statistics and resolution of the data. Theoretically, these data are compatible with both scenarios: (i) the dropping of ρ-meson mass [8] and (ii) the many-body interaction of the ρ meson with other hadrons in the nuclear medium [9]. Almost after a decade, the STAR experiment at RHIC BNL [10] found the decrease in ρ-meson mass $\sim$70 MeV in the analysis of the $\pi^+\pi^-$ production data from the peripheral Au + Au collisions. However, the upgraded CERES experiment [11] as well as the dimuon measurements (in the In-In collision) in the NA60 experiment at CERN [12] showed considerable broadening in the ρ-meson mass distribution spectrum but essentially no shift in mass.

The interpretation of the ultrarelativistic heavy-ion collision data is very complicated because this reaction occurs far from the equilibrium state, whereas the calculations for the hadronic parameters are done at normal nuclear density and zero temperature (equilibrium state). Therefore, it is more accountable to search the in-medium properties of vector meson in the normal nucleus. In fact, the modification of the vector meson is predicted to be large enough to observe it in the nuclear reaction with pion and photon beams [13]. The chiral symmetry is also shown to restore partially in the normal nucleus (specifically, inside a heavy nucleus [14]). Also, the scaling hypothesis [2] and QCD sum rule calculation [3] envisage the reduction ($\sim$15–20%) of vector meson mass in a nucleus. There also exist many-body calculations which show the drop of mass and increase in width for the vector meson in the normal nucleus [13,15]. Beside these, only width broadening [16,17], upward mass shift [18,19], and appearance of additional peaks [17,19,20] for the vector meson in the nuclear medium are predicted by various model calculations.

The modification of the vector meson in the normal nucleus has been reported by various measurements. The KEK-PS E325 collaboration at KEK [21] found the enhancement in the e^+e^- yield in the p+A reaction at 12 GeV. This enhancement is well understood due to the reduction of the vector meson mass in the nucleus. The subthreshold ρ-meson production experiment on the ^{3}He$(\gamma, \pi^+\pi^-)$X reaction, done by the TAGX Collaboration [22], reported a large decrease in the ρ meson mass. The ρ-meson polarization distribution, measured by this TAGX collaboration [23], corroborates this finding. The recent results, from Jefferson Laboratory, show the broadening of the ρ meson width in the photonuclear reaction [24]. The mass shift of the ρ meson found in this experiment is insignificant.

*swapand@barc.gov.in

Recently, the CBELSA/TAPS collaboration measured the $\pi^0\gamma$ invariant mass distribution spectrum to look for the medium modification of the ω meson in the Nb nucleus [25]. This experiment was done at the electron stretcher accelerator (ELSA) in Bonn using the tagged γ beam of energy spread $0.64 - 2.53$ GeV. The ω meson was detected through its decay $\omega \to \pi^0\gamma$. To minimize the pionic distortion on the ω meson signal, the data were taken for the π^0 meson kinetic energy T_{π^0} larger than 150 MeV. The measured spectrum for the lower ω-meson momentum k_ω bin [i.e., $200 < k_\omega(\text{MeV/c}) < 400$] shows distinct ω-meson mass modification at $\sim$730 MeV, which gradually vanishes with the increase in the ω meson momentum. However, this claim is not valid any longer [26], as a reanalysis of the data could not reproduce the spectral shape reported in Ref. [25]. The measured distributions show broad widths ($\sim$55 MeV) comparable to the resolution width of the detecting system used in the experimental setup. In fact, this width is about 6.5 times larger than the free space decay width of the ω meson ($\Gamma_\omega = 8.43$ MeV [27]). Therefore, the width of the ω meson in a nucleus Γ^*_ω can be detected in this setup if it is enhanced more than 55 MeV. The present status of this topic is summarized in the recent review articles [28].

We study microscopically the mechanism for the $(\gamma, \pi^0\gamma)$ reaction on a nucleus and compare our results with the data taken by the CBELSA/TAPS collaboration. In the energy region of this reaction, the elementary reaction occurring in the nucleus can be visualized as $\gamma N \to VN; V \to \pi^0\gamma$, where V stands for the low-energy vector mesons, that is, the ρ^0, ω, ϕ mesons. The qualitative analysis presented in Ref. [29] shows that the $\pi^0\gamma$ event in the elementary reaction arises distinctly due to the decay of the ω meson produced in the intermediate state. The contributions to this event from the ρ^0 and ϕ mesons are found negligible. Therefore, we consider that the $(\gamma, \pi^0\gamma)$ reaction on the nucleus proceeds through the formation of the ω meson in the intermediate state. The production of this meson is described by the $\gamma N \to \omega N$ reaction amplitude $f_{\gamma N\to\omega N}$, and its propagation is presented by the eikonal form. The ω-meson interaction with the nucleus (which appears in its propagator) is described by the corresponding optical potential. The decay of ω meson to π^0 and γ bosons is governed by the $\omega\pi\gamma$ Lagrangian. The π^0 meson scattering state is generated by using the π^0 meson nucleus optical potential.

II. FORMALISM

The generalized optical potential or self-energy for the photoproduction of the ω meson in a nucleus [29,30] is given by

$$\Pi_{\gamma A\to\omega A}(\mathbf{r}) = -4\pi\left[1 + \frac{E_\omega}{E_N}\right] f_{\gamma N\to\omega N}(0)\varrho(\mathbf{r}), \qquad (1)$$

where $\varrho(\mathbf{r})$ represents the spatial density distribution of the nucleus.

The factor $f_{\gamma N\to\omega N}(0)$ in Eq. (1) is the forward reaction amplitude for the elementary $\gamma N \to \omega N$ process. It is related to the four-momentum q^2 transfer distribution $d\sigma(\gamma N \to \omega N)/dq^2$ [31]:

$$\frac{d\sigma}{dq^2}(\gamma N \to \omega N; q^2 = 0) = \frac{\pi}{k_\gamma^2}|f_{\gamma N\to\omega N}(0)|^2. \qquad (2)$$

The forward $d\sigma(\gamma p \to \omega p)/dq^2$ is used to be obtained by extrapolating the measured value of $d\sigma(\gamma p \to \omega p; q^2)/dq^2$ to $q^2 = 0$. In fact, the energy-dependent values for it are reported in Refs. [31] and [32] for $E_\gamma \geqslant 1.6$ GeV. At lower energies (i.e., $E_\gamma \leqslant 2.6$ GeV), the four-momentum transfer distributions $d\sigma(\gamma p \to \omega p)/dq^2$ were measured with the SAPHIR detector at the electron stretcher ring (ELSA), Bonn [33]. We extract the energy-dependent $|f_{\gamma p\to\omega p}(0)|^2$ from the measured $d\sigma(\gamma p \to \omega p)/dq^2$, and use them in our calculation.

The ω meson, produced in the nucleus, propagates a certain distance before it decays into π^0 and γ bosons. The propagation of the ω meson from its production point $\mathbf{r}$ to its decay point $\mathbf{r}'$ can be expressed as $(-g^\mu_{\mu'} + \frac{1}{m^2}k^\mu_\omega k_{\omega,\mu'})G_\omega(m; \mathbf{r}' - \mathbf{r})$ [34]. We represent the scalar part of the ω-meson propagator $G_\omega(m; \mathbf{r}' - \mathbf{r})$ by the eikonal form [35,36], that is,

$$G_\omega(m; \mathbf{r}' - \mathbf{r}) = \delta(\mathbf{b}' - \mathbf{b})\Theta(z' - z) \times e^{i\mathbf{k}_\omega\cdot(\mathbf{r}'-\mathbf{r})} D_{\mathbf{k}_\omega}(m; \mathbf{b}, z', z). \qquad (3)$$

The factor $D_{\mathbf{k}_\omega}(m; \mathbf{b}, z', z)$ appearing in this equation describes the nuclear medium effect on the properties of the ω meson. The form for it is

$$D_{\mathbf{k}_\omega}(m; \mathbf{b}, z', z) = -\frac{i}{2k_{\omega\parallel}}\exp\left[\frac{i}{2k_{\omega\parallel}}\int_z^{z'} dz''\left\{\tilde{G}^{-1}_{0\omega}(m) - 2E_\omega V_{O\omega}(\mathbf{b}, z'')\right\}\right], \qquad (4)$$

where k_ω is the momentum of the ω meson. $V_{O\omega}(\mathbf{b}, z'')$ represents the ω-meson nucleus optical potential, which arises due to the interaction of this meson with the particles present in the nucleus. In fact, this potential modifies the hadronic parameters of the ω meson during its passage through the nucleus. $\tilde{G}_{0\omega}(m)$ denotes the ω-meson (on-shell) propagator in free space: $\tilde{G}^{-1}_{0\omega}(m) = m^2 - m^2_\omega + im_\omega\Gamma_\omega(m)$. Here, m_ω and $\Gamma_\omega(m)$ represent the resonant mass and total decay width for the ω meson, elaborated in Ref. [29].

The $\pi^0\gamma$ in the final state originates due to the decay of the ω meson (i.e., $\omega \to \pi^0\gamma$). The Lagrangian density $\mathcal{L}_{\omega\pi\gamma}$ describing this decay channel [29,37] is given by

$$\mathcal{L}_{\omega\pi\gamma} = -\frac{f_{\omega\pi\gamma}}{m_\pi}\epsilon_{\mu\nu\rho\sigma}\partial^\mu A^\nu \pi \partial^\rho \omega^\sigma, \qquad (5)$$

where $f_{\omega\pi\gamma}(= 0.095)$ denotes the $\omega\pi\gamma$ coupling constant. A^ν represents the photon field.

The wave function for photon is described by the plane wave. The distorted wave function $\chi^{(-)}(\mathbf{k}_{\pi^0}, \mathbf{r}')$ for the π^0 meson in the final state is represented by the eikonal form [35,38]:

$$\chi^{(-)*}(\mathbf{k}_{\pi^0}, \mathbf{r}') = e^{-i\mathbf{k}_{\pi^0}\cdot\mathbf{r}'} D^{(-)*}_{\mathbf{k}_{\pi^0}}(\mathbf{b}, z'). \qquad (6)$$

The factor $D^{(-)*}_{\mathbf{k}_{\pi^0}}(\mathbf{b}, z')$ in this equation describes the pionic distortion. The form for it is

$$D^{(-)*}_{\mathbf{k}_{\pi^0}}(\mathbf{b}, z') = \exp\left[-\frac{i}{v_{\pi^0\parallel}}\int_{z'}^{\infty} dz_1 V_{O\pi^0}(\mathbf{b}, z_1)\right], \qquad (7)$$

where v_{π^0} is the velocity of pion. $V_{O\pi^0}(\mathbf{b}, z_1)$ denotes the optical potential for the pion nucleus scattering in the final state.

The differential cross section for the ω meson mass m (i.e., the $\pi^0\gamma$ invariant mass) distribution can be written as

$$\frac{d\sigma(m, E_\gamma)}{dm} = \int d\Omega_\omega K_F \Gamma_{\omega\rightarrow\pi^0\gamma'}(m)|F(\mathbf{k}_\gamma, \mathbf{k}_\omega)|^2, \quad (8)$$

where K_F is the kinematical factor of the reaction. It is given by $K_F = \frac{1}{(2\pi)^3}\frac{k_\omega}{k_\gamma}m^2$, with $\mathbf{k}_\omega = \mathbf{k}_{\pi^0} + \mathbf{k}_{\gamma'}$. The prime represents the quantity in the final state.

$\Gamma_{\omega\rightarrow\pi^0\gamma}(m)$ in the above equation denotes the width for the ω meson of mass m decaying at rest into the $\pi^0\gamma$ channel. $\Gamma_{\omega\rightarrow\pi^0\gamma}(m)$ is evaluated [29] using the Lagrangian density $\mathcal{L}_{\omega\pi\gamma}$ given in Eq. (5):

$$\Gamma_{\omega\rightarrow\pi^0\gamma}(m) = \Gamma_{\omega\rightarrow\pi^0\gamma}(m_\omega)\left[\frac{k(m)}{k(m_\omega)}\right]^3, \quad (9)$$

with $\Gamma_{\omega\rightarrow\pi^0\gamma}(m_\omega = 782\ \text{MeV}) \approx 0.72$ MeV, where $k(m)$ is the momentum of pion in the $\pi^0\gamma$ center of mass system.

The factor $F(\mathbf{k}_\gamma, \mathbf{k}_\omega)$ in Eq. (8) describes the production of the ω meson in the nucleus. In addition, it also carries the information about the ω-meson propagation inside as well as outside the nucleus. The expression for it is

$$F(\mathbf{k}_\gamma, \mathbf{k}_\omega) = \int d\mathbf{r}\Pi_{\gamma A\rightarrow\omega A}(\mathbf{r})e^{i(\mathbf{k}_\gamma - \mathbf{k}_\omega).\mathbf{r}}D(\mathbf{k}_\omega; \mathbf{b}, z), \quad (10)$$

where $D(\mathbf{k}_\omega; \mathbf{b}, \mathbf{z})$ is given by

$$D(\mathbf{k}_\omega; \mathbf{b}, z) = \int_z^\infty dz' D^{(-)*}_{\mathbf{k}_{\pi^0}}(\mathbf{b}, z')D_{\mathbf{k}_\omega}(\mathbf{b}, z', z). \quad (11)$$

All quantities appearing in this equation are already defined. The ω-meson decay probabilities inside and outside the nucleus can be addressed by splitting $D(\mathbf{k}_\omega; \mathbf{b}, z)$ in Eq. (11) into two parts:

$$D(\mathbf{k}_\omega; \mathbf{b}, z) = D_{\text{in}}(\mathbf{k}_\omega; \mathbf{b}, z) + D_{\text{out}}(\mathbf{k}_\omega; \mathbf{b}, z), \quad (12)$$

where $D_{\text{in}}(\mathbf{k}_\omega; \mathbf{b}, z)$ and $D_{\text{out}}(\mathbf{k}_\omega; \mathbf{b}, z)$ describe the ω-meson decay inside and outside the nucleus respectively. Using Eq. (11), they can be written as

$$D_{\text{in}}(\mathbf{k}_\omega; \mathbf{b}, z) = \int_z^Z dz' D^{(-)*}_{\mathbf{k}_{\pi^0}}(\mathbf{b}, z')D_{\mathbf{k}_\omega}(\mathbf{b}, z', z), \quad (13)$$

$$D_{\text{out}}(\mathbf{k}_\omega; \mathbf{b}, z) = \int_Z^\infty dz' D^{(-)*}_{\mathbf{k}_{\pi^0}}(\mathbf{b}, z')D_{\mathbf{k}_\omega}(\mathbf{b}, z', z), \quad (14)$$

with $Z = \sqrt{R^2 - b^2}$. R is the extension of the nucleus. In fact, $D_{\text{out}}(\mathbf{k}_\omega; \mathbf{b}, z)$ in the above equation can be simplified to $\tilde{G}_{0\omega}(m)\exp[\frac{i}{2k_\omega}\tilde{G}^{-1}_{0\omega}(m)(Z - z)]$.

Equation (8) illustrates the differential cross section for the ω-meson mass distribution due to fixed γ-beam energy E_γ. However, as we mentioned earlier, the CBELSA/TAPS Collaboration [25] used a tagged photon beam of definite energy range in their measurement. Therefore, we modulate the cross section in Eq. (8) with the beam profile function $W(E_\gamma)$ [39]; that is,

$$\frac{d\sigma(m)}{dm} = \int_{E_\gamma^{mn}}^{E_\gamma^{mx}} dE_\gamma W(E_\gamma)\frac{d\sigma(m, E_\gamma)}{dm}. \quad (15)$$

E_γ^{mn} and E_γ^{mx} are equal to 0.64 GeV and 2.53 GeV respectively, as provided in Ref. [25]. The profile function $W(E_\gamma)$ for the γ beam (originating due to the bremsstrahlung radiation of electron impinging on the Pb target [25]) varies as $W(E_\gamma) \propto \frac{1}{E_\gamma}$ [39].

III. RESULTS AND DISCUSSION

We calculate the ω meson mass m (i.e., the $\pi^0\gamma$ invariant mass) distribution spectra in the $(\gamma, \omega \rightarrow \pi^0\gamma)$ reaction on the ^{93}Nb nucleus. The ω meson, as mentioned earlier, is detected for pion (arising due to $\omega \rightarrow \pi^0\gamma$) kinetic energy T_{π^0} greater than 150 MeV. We impose this condition in our calculation; that is, all results presented in this manuscript are calculated for $T_{\pi^0} > 150$ MeV.

The meson nucleus optical potentials [i.e., $V_{O\omega}$ in Eq. (4) and $V_{O\pi^0}$ in Eq (7)] are estimated using the $t\varrho$ approximation [35]:

$$V_{OM}(\mathbf{r}) = -\frac{v_M}{2}[i + \alpha_{MN}]\sigma_t^{MN}\varrho(\mathbf{r}). \quad (16)$$

The symbol M in this equation stands for a meson (i.e., either ω meson or π^0 meson), and N denotes a nucleon. v_M is the velocity of the meson M. α_{MN} represents the ratio of the real to imaginary part of the meson nucleon scattering amplitude f_{MN}, and σ_t^{MN} is the corresponding total cross section. Since the ω meson is a neutral unstable particle, $\alpha_{\omega N}$ and $\sigma_t^{\omega N}$ cannot be obtained directly from measurements. Lutz *et al.* [40] (using coupled-channel calculation) have estimated the energy-dependent $f_{\omega N}$ in the low-energy region, that is, $1.4 \leqslant \sqrt{s}(\text{GeV}) \leqslant 1.8$. Their calculations are well constrained by the elementary ω-meson production data in the threshold region. At higher energy, the imaginary part of $f_{\omega N}$ is extracted from the elementary ω-meson photoproduction data using the vector meson dominance model [37,41]. Sibirtsev *et al.* [41], using the additive quark model and Regge theory, have evaluated $f_{\omega N}$ for a wide range of energy. According to them, $\alpha_{\omega N}$ can be written as

$$\alpha_{\omega N} = \frac{0.173(s/s_0)^\epsilon - 2.726(s/s_0)^{-\eta}}{1.359(s/s_0)^\epsilon + 3.164(s/s_0)^{-\eta}},$$

with $s_0 = 1\text{GeV}^2$, $\epsilon = 0.08$, and $\eta = 0.45$ [41]. For $V_{O\pi^0}(\mathbf{r})$ also, the energy-dependent $\alpha_{\pi^0 N}$ and $\sigma_t^{\pi^0 N}$ cannot be measured directly. Therefore, we have worked out the π^0 meson nucleon scattering amplitude $f_{\pi^0 N}$ using isospin algebra: $f_{\pi^0 N} = \frac{1}{2}[f_{\pi^+ N} + f_{\pi^- N}]$. The energy-dependent measured values for the $\pi^\pm N$ scattering parameters (i.e., $\alpha_{\pi^\pm N}$ and $\sigma_t^{\pi^\pm N}$) are available in Ref. [42].

The nuclear-density distribution $\varrho(\mathbf{r})$ required to evaluate Eqs. (1) and (16) is approximated by the nuclear-charge-density distribution. The form of $\varrho(\mathbf{r})$ for ^{93}Nb nucleus, as obtained from the electron-scattering data, is given by

$$\varrho(\mathbf{r}) = \varrho_0\frac{1}{1 + \exp\left(\frac{r-c}{z}\right)}; \quad (17)$$

with $c = 4.87$ fm and $z = 0.573$ fm [43]. It is normalized to the mass number of the nucleus. The pair correlation (PC) in

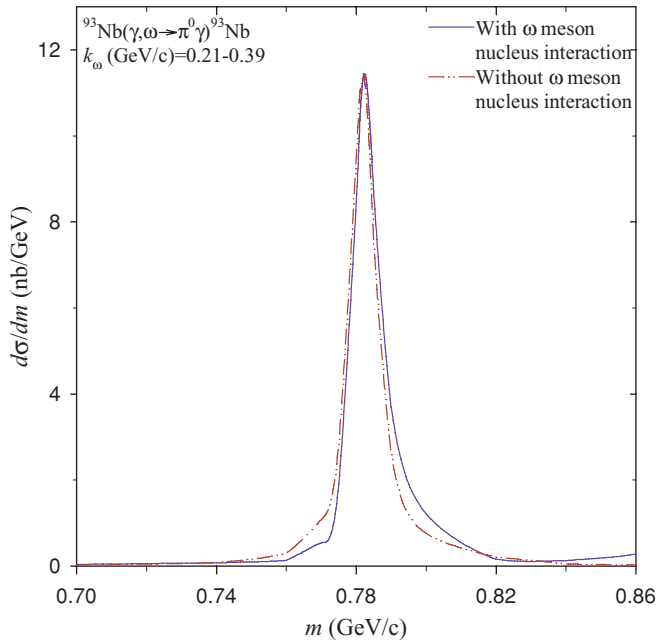

FIG. 1. (Color online) The calculated ω-meson (photoproduced in the ^{93}Nb nucleus) mass distribution spectra with (solid curve) and without (dot-dot-dashed curve) the ω-meson nucleus interaction for k_ω (GeV/c) = 0.21–0.39. The π^0 meson nucleus interaction is incorporated in both cases.

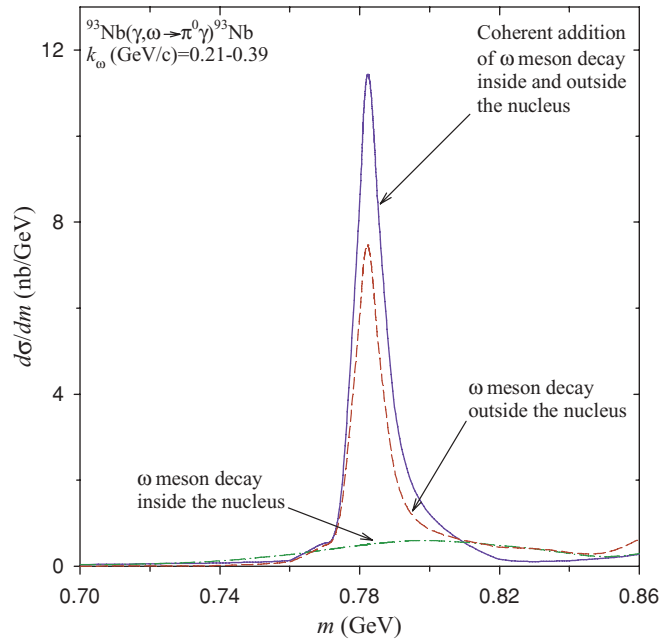

FIG. 2. (Color online) The calculated mass distribution spectra for the ω meson decaying inside as well as outside the ^{93}Nb nucleus. The dot-dashed curve represents the cross section for the ω meson decaying inside the nucleus, whereas the dashed curve corresponds to its decay outside the nucleus. The coherent addition of them is shown by the solid curve.

$\varrho(\mathbf{r})$ can be incorporated by the following replacement [30]:

$$\varrho(\mathbf{r}) \to \varrho(\mathbf{r})\left[1+\frac{1}{2}\sigma_t^{MN}\varrho(\mathbf{r})l_c\left\{\frac{\varrho(\mathbf{r})}{\varrho(0)}\right\}^{1/3}\right], \qquad (18)$$

where the correlation length l_c is equal to 0.3 fm [30]. We include α_{MN} in the above equation by the trivial substitution $\sigma_t^{MN} \to (1-i\alpha_{MN})\sigma_t^{MN}$ [38].

The onset of color transparency (CT) has been reported in many nuclear pion production reactions at intermediate energies [44,45]. The color transparency arises due to the reduction of the elementary pion nucleon total cross section over a typical length scale, commonly known as hadron formation length l_h. The standard expression for the effective cross section (which incorporates the CT effect in it [45]) is

$$\frac{\sigma_{t,\mathrm{eff}}^{\pi^0 N}}{\sigma_t^{\pi^0 N}} = \left[\left\{\frac{z}{l_h}+\frac{n^2k_t^2}{Q^2}\left(1-\frac{z}{l_h}\right)\right\}\theta(l_h-z)+\theta(z-l_h)\right]. \qquad (19)$$

The value of n is equal to 2 for a quark-antiquark color singlet system. k_t (=0.35 GeV/c) is the average transverse momentum of a quark inside the hadron; z is the straight path traveled by the pion after its formation. In the above equation, $Q^2 = |(k_\gamma^\mu - k_{\gamma'}^\mu)^2|$ and $l_h \equiv l_{\pi^0} \simeq 2k_{\pi^0}/(0.7\ \mathrm{GeV}^2)$ [45].

The main purpose of this calculation is to look for the in-medium properties of ω meson in the nucleus. We, therefore, present in Fig. 1 the ω-meson mass distribution spectra calculated with and without the ω-meson nucleus (i.e., Nb nucleus) interaction for k_ω (GeV/c) = 0.21–0.39. As mentioned earlier, it is the lowest ω-meson momentum bin in the measurement where the medium modification was shown to occur [25]. The solid curve in Fig. 1 represents the previous case, that is, the ω-meson nucleus interaction is incorporated in the calculated cross section. The cross section calculated without this interaction is presented by the dot-dot-dashed curve. In both cases, the pion nucleus interaction has been incorporated. This figure distinctly shows the absence of medium modification for the ω meson photoproduced in the Nb nucleus for $0.2 < k_\omega$ (GeV/c) < 0.4.

Since Fig. 1 does not show the medium modification of the ω meson produced in the Nb nucleus, we envisage comparing the ω-meson decay probabilities inside and outside the nucleus for the same kinematical condition quoted in Fig. 1, that is, $0.2 < k_\omega$ (GeV/c) < 0.4. In Fig. 2, we plot the mass distribution spectra for the ω meson decaying inside and outside the Nb nucleus. This figure shows that the ω meson decays dominantly outside the nucleus (dashed curve). The cross section for the ω meson decaying inside the nucleus is presented by the dot-dashed curve. The solid curve in Fig. 2 illustrates that the coherent addition of the amplitudes of the ω meson decaying inside and outside the nucleus enhances the cross section significantly at the peak. For $k_\omega > 0.4$ GeV/c, the ω meson moves faster, resulting in less interaction with the nucleus. In such cases, the cross section for the ω meson decaying outside the nucleus would be relatively larger than that shown in Fig. 2. Therefore, the medium effect on the ω meson in the Nb nucleus is hardly possible under these circumstances.

It should be mentioned that the ω meson decays throughout its passage inside as well as outside the nucleus. The decay probability of this meson inside the nucleus would be larger

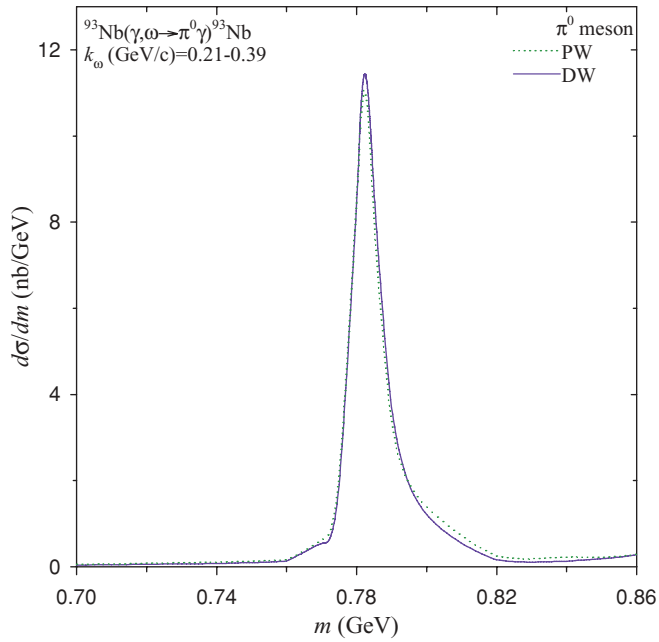

FIG. 3. (Color online) The effect of pionic distortion on the ω-meson mass distribution spectrum for k_ω (GeV/c) = 0.21–0.39. The dotted curve represents the calculated spectrum where the plane wave for π^0 meson is considered in the calculation. The incorporation of the pionic distortion, as shown by the solid curve, hardly alters the plane wave result.

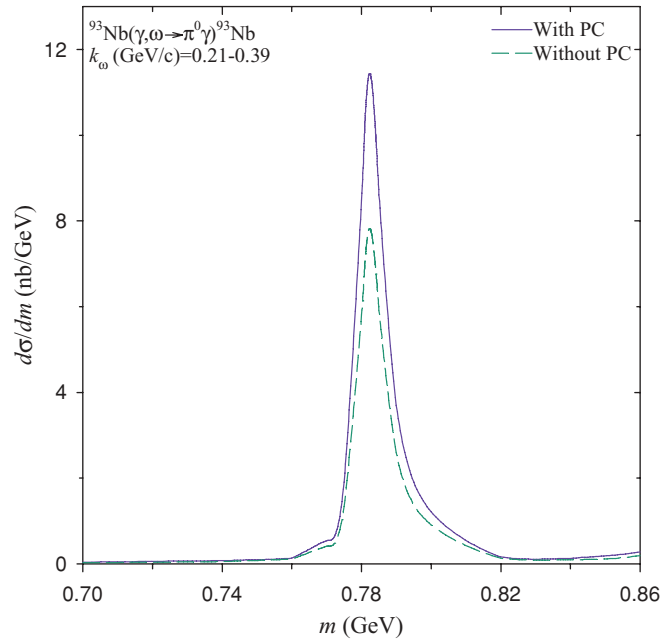

FIG. 4. (Color online) The sensitivity of the pair correlation (PC) on the ω-meson mass distribution spectrum. The solid and dashed curves describe respectively the calculated cross sections with and without PC incorporated in the nuclear density distribution (see text).

if its effective decay length $L^*_\omega (= v_\omega/\Gamma^*_\omega)$ in the nucleus is less than the dimension of the nucleus. Here, v_ω and Γ^*_ω denote the velocity and the effective width of the ω meson in the nucleus. Since the width of the ω meson in the free state (i.e., Γ_ω) is equal to 8.43 MeV, the free-space ω meson decay length $L_\omega (= v_\omega/\Gamma_\omega)$ is about 5.8 fm for k_ω equal to 200 MeV/c. This decay length would be much larger for k_ω equal to 400 MeV/c ($L_\omega \sim 10.66$ fm for $k_\omega = 400$ MeV/c). Therefore, L_ω for $k_\omega = 200$-400 MeV is significantly larger than the radius of the ^{93}Nb nucleus ($R_{\rm rms} \sim 4.3$ fm). The above analysis shows that the ω meson cannot decay inside the Nb nucleus unless its width in this nucleus is drastically increased (i.e., $\Gamma^*_\omega \gg \Gamma_\omega$).

We present in Fig. 3 the calculated results showing the effect of pionic distortion on the ω-meson mass distribution spectrum for $0.2 < k_\omega$ (GeV/c) < 0.4. This figure shows that the calculated cross section is not sensitive to the pion nucleus interaction. The decay of the ω meson ($\rightarrow \pi^0\gamma$) predominantly outside the nucleus (shown in Fig. 2) causes the cross section to be insensitive to this interaction. The incorporation of CT in the pion nucleus interaction [see Eq. (19)] does not make any change in the calculated spectrum. Therefore, we do not show it. In fact, the cross section, as mentioned above, is not sensitive to the pion nucleus interaction itself. It could be added that CT is a high-energy phenomenon (i.e., $Q^2 \geqslant 1$). Large hadron formation length l_h (which occurs at higher pion momentum) is also needed for the color transparency. Therefore, CT is not expected in the low-energy nuclear reaction, as considered in this paper.

The sensitivity of the PC to the calculated cross section is presented in Fig. 4. The solid curve in this figure shows the calculated ω-meson mass distribution spectrum where PC is included in the nuclear density distribution [see $\varrho(\mathbf{r})$ in Eqs. (17) and (18)]. The dashed curve represents the calculated spectrum without PC incorporated in the nuclear density distribution, that is, $\varrho(\mathbf{r})$ given in Eq. (17). Note that PC is included in all other results shown in this paper. Figure 4 shows that the incorporation of PC increases the magnitude of the calculated cross section significantly (i.e., by a factor of $\sim$ 1.46 at the peak).

The broad width appearing in the measured $\pi^0\gamma$ invariant mass distribution spectra is presumably due to the large resolution width ($\sim$55 MeV) in the detecting system used in the experimental setup [25]. We incorporate this in our formalism by folding a Gaussian function $R(m, m')$ with the differential cross section given in Eq. (15), that is,

$$\frac{d\sigma(m)}{dm} = \int dm' R(m, m') \frac{d\sigma(m')}{dm'}. \tag{20}$$

The function $R(m, m')$ in this equation accounts for the resolution width for the detector used in the measurement. It is given by

$$R(m, m') = \frac{1}{\sigma\sqrt{2\pi}} e^{-(m-m')^2/2\sigma^2}, \tag{21}$$

where σ is related to the full width at half-maxima (FWHM) of the resolution function $R(m, m')$: FWHM $= 2.35\sigma$ [46]. The value of FWHM is taken equal to the width of the detector resolution, that is, 55 MeV as given in Ref. [25]. Figure 5 shows that the incorporation of the detector resolution function in the calculation reduces the cross section at the

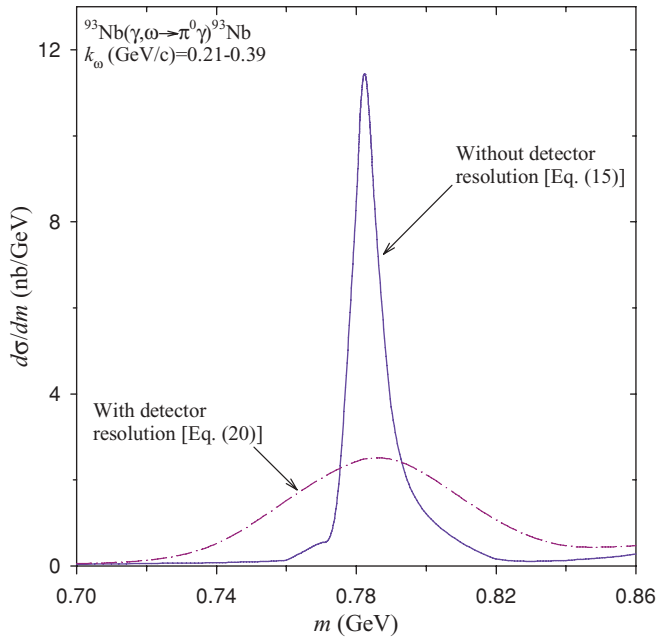

FIG. 5. (Color online) The effect of the detector resolution on the ω-meson mass distribution spectrum. The solid curve corresponds to the cross section given in Eq. (15), where the detector resolution is not incorporated in the calculation. The dot-dashed curve represents the cross section where the detector resolution is incorporated in the calculation; see Eq. (20) in the text.

peak, and it simultaneously enhances the width of the cross section.

We present in Fig. 6 the calculated results due to Eq. (20) along with the measured $\pi^0\gamma$ invariant mass distribution spectra (histograms, taken from the Ref. [25]) for the ω-meson momentum bins: (i) $0.6 < k_\omega$ (GeV/c) < 1 and (ii) $1 < k_\omega$ (GeV/c) < 1.4. The solid curves appearing in this figure denote the calculated spectra for (i) $k_\omega = 0.61 - 0.99$ GeV/c and (ii) $k_\omega = 1.01 - 1.39$ GeV/c. It is noticeable in this figure that the calculated distributions reproduce the data very well. As mentioned earlier, the CB/TAPS Collaboration reported the modification of ω-meson mass in the Nb nucleus in the region below 780 MeV for $0.2 < k_\omega$ (GeV/c) < 0.4 and $0.4 < k_\omega$ (GeV/c) < 0.6 [25]. Since this claim is no longer valid [26], we do not compare the calculated results with the data for $k_\omega < 0.6$ GeV/c.

IV. CONCLUSIONS

We have studied the mechanism for the $(\gamma, \pi^0\gamma)$ reaction on Nb nucleus in the energy region 0.64–2.54 GeV. The π^0 and γ bosons appearing in coincidence in the final state are shown to originate from the decay of ω meson produced in the intermediate state. The calculated results show that the properties of ω meson in the nucleus are not modified for the kinematics used in the measurement done at ELSA. This occurs since the ω meson predominantly decays outside the nucleus. This is also the reason for not showing the distortion due to final-state interaction, that is, the π^0 meson-nucleus interaction. The incorporation of color transparency in the pion nucleus interaction does not change the cross section for the

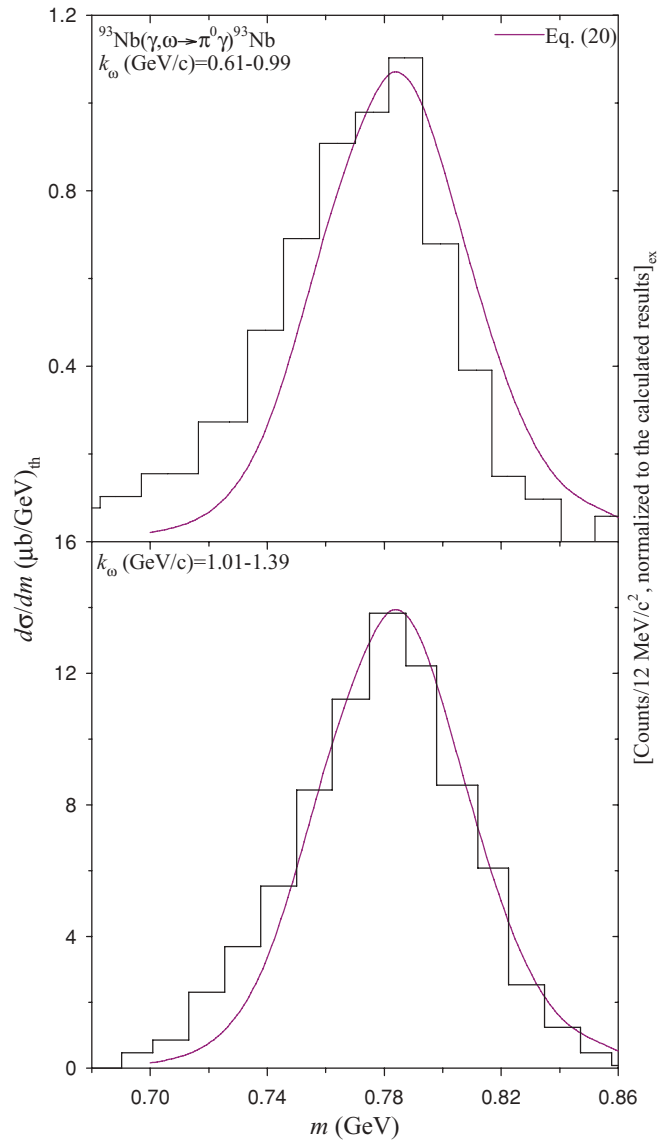

FIG. 6. (Color online) The calculated ω-meson mass distribution spectra [solid curves due to Eq. (20)] in the $(\gamma, \omega \to \pi^0\gamma)$ reaction on ^{93}Nb nucleus for the ω-meson momentum bins quoted in the figure. The histograms represent the measured $\pi^0\gamma$ invariant mass distribution spectra (taken from Ref. [25]), normalized to the calculated cross sections.

ω-meson mass distribution. The inclusion of pair correlation in the nuclear density distribution increases the magnitude of the cross section. The broad width in the measured distribution is found to arise due to the large resolution width associated with the detector used in the experiment. The calculated results reproduce the measured spectra very well.

ACKNOWLEDGMENTS

I gratefully acknowledge Dr. L. M. Pant for making me aware of the measurement for the ω-meson mass distribution. The communication with Dr. E. Oset regarding the beam profile function was very helpful. The discussion with Dr. D. R. Chakrabarty on the detector resolution is highly appreciated.

[1] C. M. Ko, V. Koch, and G. Li, Annu. Rev. Nucl. Part. Sci. **47**, 505 (1997); W. Cassing and E. L. Bratkovskaya, Phys. Rep. **308**, 65 (1999); R. Rapp and J. Wambach, Adv. Nucl. Phys. **25**, 1 (2000).

[2] G. E. Brown and M. Rho, Phys. Rev. Lett. **66**, 2720 (1991).

[3] T. Hatsuda and S. H. Lee, Phys. Rev. C **46**, R34 (1992).

[4] M. Asakawa, C. M. Ko, P. Levai, and X. J. Qiu, Phys. Rev. C **46**, R1159 (1992); M. Asakawa and C. M. Ko, *ibid.* **48**, R526 (1993); Nucl. Phys. A **560**, 399 (1993).

[5] K. Saito, K. Tsushima, and A. W. Thomas, Phys. Rev. C **55**, 2637 (1997).

[6] M. Urban, M. Buballa, R. Rapp, and J. Wambach, Nucl. Phys. A **673**, 357 (2000).

[7] A. Drees, Nucl. Phys. A **610**, 536c (1996); Th. Ullrich (CERES Collaboration), *ibid.* **610**, 317c (1996); M. Masera (HELIOS-3 Collaboration), *ibid.* **590**, 93c (1995); E. Scomparin (NA50 Collaboration), *ibid.* **610**, 331c (1996).

[8] G. Q. Li, C. M. Ko, and G. E. Brown, Phys. Rev. Lett. **75**, 4007 (1995); G. Q. Li, C. M. Ko, G. E. Brown, and H. Sorge, Nucl. Phys. A **611**, 539 (1996); W. Cassing, W. Ehehalt, and C. M. Ko, Phys. Lett. B **363**, 35 (1995); W. Cassing, W. Ehehalt, and I. Karlik, *ibid.* **377**, 5 (1996).

[9] G. Chanfray, R. Rapp, and J. Wambach, Phys. Rev. Lett. **76**, 368 (1996); R. Rapp, G. Chanfray, and J. Wambach, Nucl. Phys. A **617**, 472 (1997); W. Cassing, E. L. Bratkovskaya, R. Rapp, and J. Wambach, Phys. Rev. C **57**, 916 (1998); R. Rapp and J. Wambach, Eur. Phys. J. A **6**, 415 (1999); T. Renk, R. Schneider, and W. Weise, Phys. Rev. C **66**, 014902 (2002).

[10] J. Adams *et al.*, Phys. Rev. Lett. **92**, 092301 (2004).

[11] D. Adamová *et al.*, Phys. Lett. B **666**, 425 (2008).

[12] R. Arnaldi *et al.*, Phys. Rev. Lett. **96**, 162302 (2006); Eur. Phys. J. C **49**, 235 (2007); S. Damjanovic *et al.*, Nucl. Phys. A **783**, 327c (2007).

[13] M. Effenberger, E. L. Bratkovskaya, and U. Mosel, Phys. Rev. C **60**, 044614 (1999); Th. Weidmann, E. L. Bratkovskaya, W. Cassing, and U. Mosel, *ibid.* **59**, 919 (1999); M. Effenberger, E. L. Bratkovskaya, W. Cassing, and U. Mosel, *ibid.* **60**, 027601 (1999).

[14] M. C. Birse, J. Phys. G: Nucl. Part. Phys. **20**, 1537 (1994).

[15] F. Klingl *et al.*, Z. Phys. A **356**, 193 (1996); Nucl. Phys. A **650**, 299 (1999).

[16] D. Cabrera and M. J. Vicente Vacas, Phys. Rev. C **67**, 045203 (2003); D. Cabrera, L. Roca, E. Oset, H. Toki, and M. J. Vicente Vacas, Nucl. Phys. A **733**, 130 (2004); V. K. Magas, L. Roca, and E. Oset, Phys. Rev. C **71**, 065202 (2005).

[17] M. Herrmann, B. L. Friman, and W. Nörenberg, Z. Phys. A **343**, 119 (1992); Nucl. Phys. A **560**, 411 (1993).

[18] A. K. Dutt-Mazumder, R. Hoffman, and M. Pospelov, Phys. Rev. C **63**, 015204 (2000); S. Zschocke, O. P. Pavlenko, and B. Kamper, Phys. Lett. B **562**, 57 (2003).

[19] D. Cabrera, E. Oset, and M. J. Vicente Vacas, Nucl. Phys. A **705**, 90 (2002).

[20] M. Post, S. Leupold, and U. Mosel, Nucl. Phys. A **741**, 81 (2004).

[21] R. Muto *et al.*, J. Phys. G: Nucl. Part. Phys. **30**, S1023 (2004); M. Nakuri *et al.*, Phys. Rev. Lett. **96**, 092301 (2006); R. Muto *et al.* (KEK-PS E325 Collaboration), *ibid.* **98**, 042501 (2007).

[22] G. J. Lolos *et al.*, Phys. Rev. Lett. **80**, 241 (1998).

[23] G. M. Huber *et al.* (TAGX Collaboration), Phys. Rev. C **68**, 065202 (2003).

[24] R. Nasseripour *et al.* (CLAS Collaboration), Phys. Rev. Lett. **99**, 262302 (2007); M. H. Wood *et al.* (CLAS Collaboration), Phys. Rev. C **78**, 015201 (2008).

[25] D. Trnka *et al.* (CBELSA/TAPS Collaboration), Phys. Rev. Lett. **94**, 192303 (2005).

[26] M. Nanova *et al.*, Phys. Rev. C **82**, 035209 (2010); Eur. Phys. J. A **47** 16 (2011); V. Metag (private communication).

[27] R. M. Barnett *et al.*, Particle Data Group, Phys. Rev. D **54**, 333 (1996).

[28] S. Leupold, V. Metag, and U. Mosel, Int. J. Mod. Phys. E **19**, 147 (2010); arXiv:0907.2388 [nucl-th]; R. S. Hayano and T. Hatsuda, Rev. Mod. Phys. **82**, 2949 (2010).

[29] S. Das, Phys. Rev. C **78**, 045210 (2008).

[30] A. Pautz and G. Shaw, Phys. Rev. C **57**, 2648 (1998).

[31] A. Sibirtsev, H.-W. Hammer, U.-G. Meißner, and A. W. Thomas, Eur. Phys. J. A **29**, 209 (2006).

[32] A. Sibirtsev, K. Tsushima, and S. Krewald, Phys. Rev. C **67**, 055201 (2003).

[33] J. Barth *et al.*, Eur. Phys. J. A **18**, 117 (2003).

[34] S. Das, Pramana **75**, 665 (2010).

[35] S. Das, Phys. Rev. C **72**, 064619 (2005).

[36] Ye. S. Golubeva, L. A. Kondratyuk, and W. Cassing, Nucl. Phys. A **625**, 832 (1997).

[37] G. I. Lykasov, W. Cassing, A. Sibirtsev, and M. V. Rzjanin, Eur. Phys. J. A **6**, 71 (1999).

[38] R. J. Glauber, in *Lectures in Theoretical Physics*, edited by W. E. Brittin *et al.*, Vol. 1 (Interscience Publishers, New York, 1959), p. 315.

[39] M. Kaskulov, E. Hernandez, and E. Oset, Eur. Phys. J. A **31**, 245 (2007).

[40] M. F. M. Lutz, Gy. Wolf, and B. Friman, Nucl. Phys. A **706**, 431 (2002).

[41] A. Sibirtsev, Ch. Elster, and J. Speth, arXiv:nucl-th/0203044.

[42] R. M. Barnett *et al.*, Particle Data Group, Phys. Rev. D **54**, 192 (1996); [http://pdg.lbl.gov/xsect/contents.html].

[43] C. W. De Jager, H. De Vries, and C. De Vries, At. Data Nucl. Data Tables **14**, 479 (1974).

[44] B. Clasie *et al.*, Phys. Rev. Lett. **99**, 242502 (2007).

[45] W. Cosyn, M. C. Martínez, J. Ryckebusch, and B. Van Overmeire, Phys. Rev. C **74**, 062201(R) (2006); A. Larson, G. A. Miller, and M. Strikman, *ibid.* **74**, 018201 (2006); G. R. Farrar, H. Liu, L. L. Frankfurt, and M. I. Strikman, Phys. Rev. Lett. **61**, 686 (1988).

[46] G. F. Knoll, *Radiation Detection and Measurement* (John Wiley & Sons, New York, 1989), p. 116.